Electrostatic Assembly of Alumina Nanoparticles on Nanocrystalline Diamond Films

E. Verveniotis, A. Kromka, and B. Rezek
Institute of Physics ASCR, Cukrovarnicka 10, Prague 6, Czech Republic.

Abstract. We apply atomic force microscope for local electrostatic charging of oxygen-terminated nanocrystalline diamond (NCD) thin films deposited on silicon, to induce electrostatically driven self-assembly of colloidal alumina nanoparticles into micro-patterns. The NCD films have sub-100 nm thickness and 60% relative sp^2 phase content. We characterize charge contrast and stability in air, fluorocarbon oil and water by Kelvin force microscopy. We discuss factors influencing the charging process and demonstrate that the contrast of more than ± 1 V is needed to induce self-assembly of the nanoparticles via coulombic and polarization forces.

Introduction

Electrostatic charging of surfaces is widely used in a variety of technological processes. It improves wetting of plastics for painting, it is employed in electronics, e.g., in detectors or memory devices, and it is used in printers and copiers for toner positioning on paper. In this context electrostatic charging has been also explored as an effective method for guiding self-assembly of micro- and nanosized elements on insulating materials [1–3]. Electrostatic charging can be generated by various methods (laser, ion, or electron beam illumination, diverse electrodes, etc.). Charged patterns of sub-micrometer dimensions can be created using nanometer-sized probes, such as those employed in atomic force microscopy (AFM) [4, 5].

A large variety of materials have been applied for electrostatic charge storage: semiconductors [4] including amorphous silicon [5] as well as dielectric materials such as polytetrafluoroethylene and poly(methyl methacrylate) [6]. Detection and understanding of electrostatic charging of diamond is crucial for many diamond-based electronic applications from detectors to field-effect transistors, batteries, silicon on diamond systems as well as for electrostatically-guided assembly. This is because diamond as a semiconductor material can, for instance, be used for device fabrication [7], for passive and active bio-interfaces [8, 9], and can be deposited on diverse substrates in nanocrystalline form [10]. From the electronic point of view, diamond is a wide band gap semiconductor (5.5 eV). Nevertheless, it can be transformed into p- or n-type semiconductor by boron [11] or phosphorus [12] doping, respectively. Intrinsic diamond is generally electrically insulating and transparent for visible light. Only when the intrinsic diamond is hydrogen-terminated (H-diamond), a thin (<10 nm) conductive layer is formed close to the diamond surface (surface conductivity) under ambient conditions [13]. While this feature attracted considerable interest and research effort in the past [14], research on electronic properties of highly resistive oxygen-terminated intrinsic diamond (O-diamond) has been limited. It was related mostly to applications in radiation detectors [15], UV detectors [16], or field-effect transistors [17, 18].

As regards local and intentional electrostatic charging, diamond has been only little investigated [19–22] even though it exhibits a unique set of properties for applications as described above. Both positive and negative persistent potential changes were observed on nanocrystalline diamond (NCD) by Kelvin force microscopy (KFM) [19], unlike in silicon thin films [5]. This has been attributed to the capacitor-like behavior of the NCD films [19]. Comparing charging of NCD films prepared on gold [19] and silicon [20] substrates demonstrates that the charging is not due to the substrate itself as could be argued in the case of silicon substrates. The charging has been also shown to be more effective when the NCD films contain more sp^2 phase [21]. Yet maximal induced electrostatic potential contrast has been reported to vary depending on a position on the sample [22]. This may depend on the local material properties, charge stability as well as actual tip condition.

Thus, in this work, we apply AFM and KFM to study local electrostatic charging of oxygen-terminated NCD films with sub-100 nm thickness and 60% relative sp^2 phase content. We characterize charge contrast and stability in air, fluorocarbon oil and water and identify the threshold for inducing electrostatic self-assembly of colloidal nanoparticles into micro-patterns.

Materials and Methods

NCD films were prepared by microwave plasma chemical vapor deposition using the following parameters: substrate temperature 820°C, deposition time 16 minutes, microwave plasma power 900 W, CH_4:H_2 dilution 3:300. Resulting thickness was 74 nm as measured by ellipsometry. The substrates were 5×10 mm^2 conductive

p-doped silicon wafers nucleated by water-dispersed detonation diamond powder of 5 nm nominal particle size (NanoAmando, New Metals and Chemicals Corp. Ltd., Kyobashi) using an ultrasonic treatment for 40 min. After the deposition, the diamond films were oxidized in r.f. oxygen plasma (300 W, 3 min) [23]. Raman spectroscopy showed 60% relative sp^2 phase content in the films [22].

Localized charging was performed by scanning in contact mode with an atomic force microscope (N-TEGRA system by NT-MDT). Conductive, diamond coated silicon probes were used (DCP11 by NT-MDT). Applied contact forces were ≈ 100 nN. The bias voltage was applied to the tip while the silicon substrates were grounded. An external voltage amplifier (HP 6826A) was connected to the cantilever and controlled by the AFM software via a signal access module, to apply voltages within the range of ± 25 V (the potential contrast is saturated at these voltages [20]). The scan speed was always 10 μm/s. Kelvin Force microscopy (KFM) was then used to detect potential differences across the sample [24]. The charged patterns are rectangles whose size depends on each experiment. Dimensions of each rectangle (charged stripe) is typically 1×8 μm or 1×2 μm unless otherwise noted. The KFM potential values and differences are given here as measured, not with respect to the vacuum level. Relative humidity and temperature during all AFM experiments were in the ranges of 20–32 % and 22–26 °C.

For achieving directed self-assembly of nanoparticles, a charged sample was immersed vertically into a colloidal emulsion for 10 sec. The sample was then let to dry in air for 5 min. The emulsion was prepared by putting 300–500 μl of the aqueous suspension containing the nanoparticles (alumina of 50 nm nominal size, Buehler, U.S.A.) into 5 ml of an insulating fluorocarbon oil (Fluorinert FC-77, 3M Company, USA) and ultra-sonicating the mixture for 20 sec. Since the two liquids do not mix, ultrasonication provided the means for creating emulsion with microscopic colloidal droplets [3]. FC-77 was selected due to its inertness, letting the charged features to maintain their electrical potential even after immersion, and allowing electrostatic forces to reach relatively far into the emulsion (>> 1 μm).

Results

The maximum achievable potential shift in each polarity was varying when the experiment was repeated (inherently at another position on the sample). This is illustrated in Figure 1, where we can see the total potential contrast varying from 230 to 2000 mV. The data points correspond to average potential within the individual stripes that were charged using the same experimental parameters. The x-axis values between two integer values correspond to experiments conducted within the same day. Positive and negative data points at the same x-value were obtained from a charging experiment and KFM in one scan frame. Only in the case of x=8 the patterns were charged in separate frames. This was also the only instance where we were able to assemble nanoparticles on the charged features. The experiments were conducted within one year. The x-scale is not linear and time between experiments is not fixed. However, the graph shows true sequence of experiments.

AFM topography of our NCD film after charging with –25 V and +25 V is shown in Figures 2a and 3a, respectively. It does not indicate any structural alteration on the sample after charging. The corresponding KFM images of the charged patterns are shown in Figures 2b and 3b. The dimensions of the cross arms are 10×80 μm.

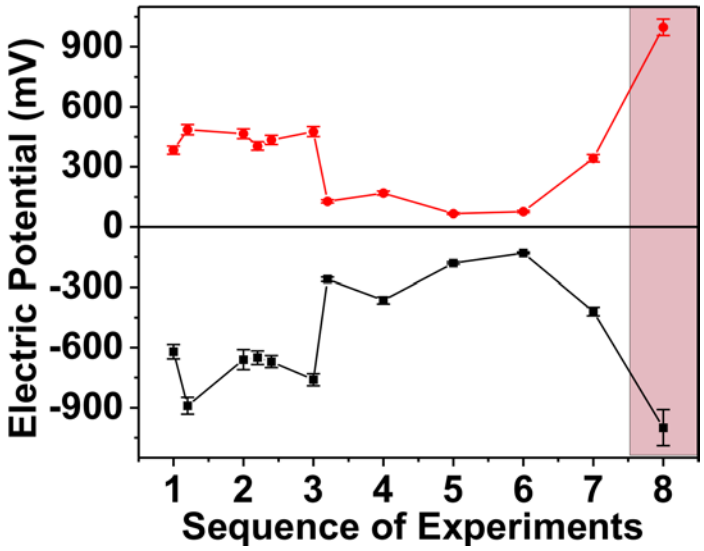

Figure 1. Surface potential shifts after electrostatic charging for positive and negative polarity. The x-axis values between two integer values correspond to experiments conducted within the same day. Shadowed region indicates the case where consequent self-assembly of nanoparticles was successful.

Maximum amplitude of the charged patterns is 1.2 V (average = 1 V) in each polarity. The centers of the crosses show slightly higher potential compared to the rest because they were charged twice (horizontally and vertically). The potential is not double, though, since the charging exhibits saturation as reported before [20]. It is also noticeable that the induced charge is not homogeneous within the charged feature (cross). The top component of the cross in Figure 2b, together with a small area of the left component near the center of the cross exhibit up to double the electric potential compared to the rest of the features (1.2 V vs. 0.6 V). In addition, we see several non- or weakly charged areas in the right component. Similarly, in the cross charged with positive voltage we can identify brighter (e. g. top left region) and darker (lower cross component) areas indicating non-homogeneous charging as well.

In Figures 2c and 3c one can see optical microscope images of the charged crosses after immersion to the solution containing the alumina nanoparticles. The nanoparticles assembled preferentially on the crosses. Their arrangement is determined by the polarity of the particular charged cross. Negative potential produced a filling effect, where the assembly occurred on the charged area. Positive potential lead to a decorative effect with the nanoparticles being attached predominantly on the pattern edges. Charged patterns having potential contrast below 1 V did not lead to preferential assembly of the nanoparticles.

Local topography and KFM maps of the charged crosses after assembly can be seen in Figures 2d,e and 3d,e. The morphology is correlating with the optical microscope images where we can identify several clusters of the assembled nanoparticles. However, KFM maps after assembly appear with doubled potential compared to the state prior to the self-assembly. The effect of solution on the charge contrast was therefore investigated more systematically.

Figure 4 illustrates the electric potential decay of features charged with ± 25 V after the sample interaction with various liquids. The data spots in x=1 correspond to the potential detected after charging in air. Then we measured the potential of the same features after immersing the sample in a) FC77 (x = 2), b) the self assembly emulsion (x=3) and c) pure de-ionized water (x=4). We can see that after each step the charged potential drops, but this decay is in the limits of what has been observed before concerning charge temporal stability in ambient conditions [19].

Discussion

In order to generate self-assembly of nanoparticles on charged areas, the electrostatic forces must be high enough to attract particles from the solution and promote assembly. In various charging instances with charged potential up to 800 mV the self-assembly was not possible. Therefore we deduce that potential differences below 1 V are insufficient to generate the self-assembly. This is corroborated with reports of a-Si:H charging, where contrast up to 0.8 V was not sufficient for self assembly [25]. Therefore, we believe that the threshold for assembly (1 V) is not a material-related issue but rather an absolute number representing the minimum electrostatic field intensity necessary for promoting the self-assembly. This means that the proposed threshold may be applicable on any material subjected to this methodology.

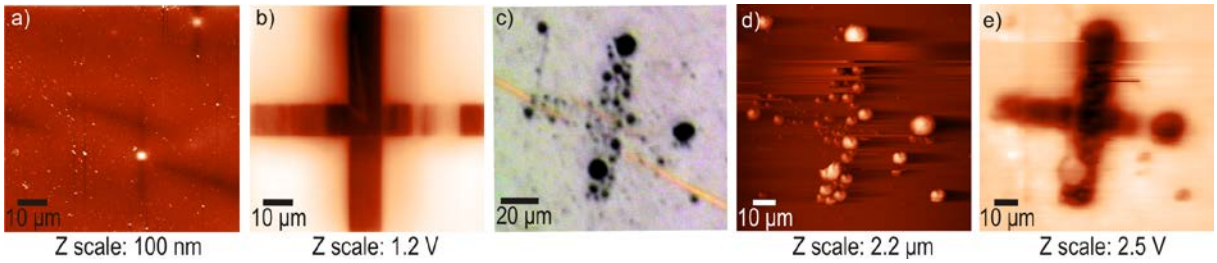

Figure 2. AFM topography on negatively charged areas (a) before and (d) after nanoparticle assembly. (b,e) Corresponding KFM potential maps. (c) Optical microscope image of the charged cross after assembly.

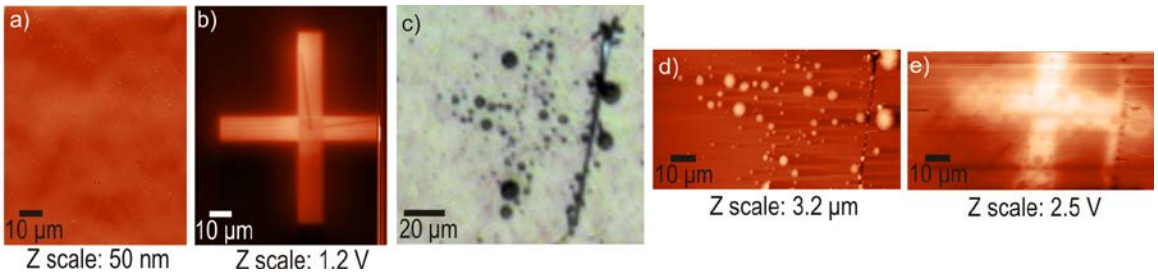

Figure 3. AFM topography on positively charged areas (a) before and (d) after nanoparticle assembly. (b,e) Corresponding KFM potential maps. (c) Optical microscope image of the charged cross after assembly.

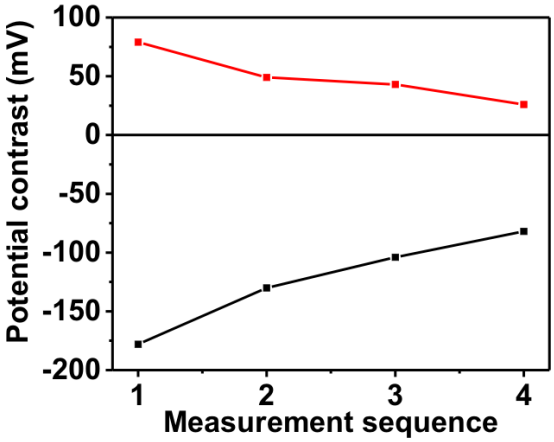

Figure 4. Surface potential evolution after immersion of the charged samples to different solutions: 1—initial, 2—fluorocarbon oil, 3—colloidal emulsion, 4—de-ionized water.

The contrast of 1.2 V vs. the uncharged background was already sufficient to generate self-assembled patterns on nanocrystalline diamond even though it is still considerably lower than the potentials typically used in the case of dielectric materials (3–5 V) [1–3]. The density of assembled nanoparticles is higher in the upper component of the cross in Figure 2b as it exhibits slightly higher potential compared to the other two components on which the nanoparticles assembled. Furthermore, the nanoparticles are missing in one region in the right component of the same cross where the charge contrast was lower (600 mV). Combination of positively and negatively charged regions may improve definition of the self-assembled pattern but it will not increase the electrostatic force itself needed for assembly. Hence the properties and charging process of NCD film have to be optimized to achieve contrast ≥ 1 V versus surrounding surface of the film.

The different style of nanoparticle assembly as a function of charge contrast polarity can be explained from the fact that the nominally uncharged nanoparticles got positively charged (including their aqueous shell around them) when emulsified in the FC-77. This is due to the relative dielectric constant ε_r difference between the materials (9.9 vs. 1.86), as materials with higher ε_r tend to charge positively when brought in contact with other materials having lower ε_r [3]. Hence, the positively charged nanoparticles cover negatively charged areas via coulomb interaction. The edge decoration observed in Figure 3c is due to attachment of non-charged or weakly charged nanoparticles that are attracted via polarization effects to the places exhibiting the highest electrostatic field gradient. Positively charged particles are repelled from the interior of the pattern.

Even though there are numerous forces acting on the nanoparticles, our methodology helps minimize their impact to the assembly process. For example, the charged sample is immersed in the emulsion immediately after the ultrasonic treatment of the latter (thus avoiding ultrasonic agitation present in [3]). Hence, there is no relaxation time so there is no accumulation of particles floating on the surface or sitting on the bottom of the beaker, influenced by gravitational forces (i.e. the emulsion is relatively homogeneous at exposure time). Therefore, it is clear that coulomb forces and polarization dominate our system irrespective of the polarity of the induced electrostatic field.

From Figure 4 we can see that immersing the charged sample into oil and water based solutions does not affect the charge more than the ambient air. Note that immersion to water did not completely neutralize the charge in NCD. Similar effect was observed also on charged a-Si:H thin films [25]. It is unlike in polymers or SiO_2 [3], indicating that the observed potential contrast arises also from the bulk of the diamond film and does not occur merely due to charge trapping in surface states. In addition, interaction between the sample and the nanoparticle emulsion was not confirmed to be responsible for the doubled potential observed after the self assembly. This could be due to some experimental artifact or unknown effect that still needs to be resolved.

There are various factors that can influence the charging and lead to the observed potential contrast variations in different experiments/positions under otherwise same experimental conditions. The first factor is ambient environment. Humidity can affect the size of the meniscus formed between the AFM tip and the sample while scanning under ambient conditions [26]. This can influence the area over which the voltage is applied, possibly altering electric field and current density, current path, as well as capacitance. Ambient temperature variations may also influence the electrical behavior of the system by moving the conduction threshold [27]. However, in our case, relative humidity and temperature was within 12 % and 4°C respectively. This range is unlikely to cause significant effect.

Morphology of the diamond film may also play a role. In our samples the surface morphology was relatively flat (5 nm RMS) and uniform. But that may not be so in the film volume. As the relative sp^2 content of

the charged film is believed to be the governing factor towards effective charging [21], local accumulation of very small grains under the surface on the specific area being charged may lead to an increase in the local sp^2 content (more grain boundaries). This could increase the potential contrast. Nevertheless, local material differences based on the micro-Raman spectra are within 2 % of relative sp^2 content [22]. We assume that this is not enough to explain variation by almost an order of magnitude in the potential contrast.

Another factor to consider is a quality of the tip-sample junction. An AFM tip can be abraded due to scanning. This could lead to local removal of the conductive-diamond coating of the tip, bringing the sample in contact with the residual SiO_2 at the very tip end [28]. This may cause a drop in the applied voltage, which would result in lower voltage across the diamond itself. However, that would cause monotonous decrease in potential contrast which is not observed in Figure 1. Still, the quality of the electrical junction can be fluctuating during scanning, in particular on corrugated surface [29]. Such effects would be in agreement with line-based fluctuations of the charge contrast as observed in Figure 2. Hence the tip-surface junction may be the most important factor.

In spite of the above mentioned problems, we were able to demonstrate the feasibility of self-assembly on diamond. Understanding and systematically achieving high charging contrast on NCD films is a matter of further research.

Conclusions

By experimenting with local electrostatic charging of nanocrystalline diamond we have attributed variations in the potential (charge) contrast mainly to the changing quality of tip-surface junction. Based on charge stability in diverse solutions we have deduced that the charge is stored not only on the surface but also in the bulk of the film. We have demonstrated successful electrostatically guided self-assembly of alumina nanoparticles into micro-patterns on NCD thin films and found that charge contrast must be $\geq \pm 1$ V in order to generate the self-assembly. These findings may be useful for better understanding and control of electrostatic charging of diamond and its potential use for guided self-assembly of nanoscale objects.

Acknowledgements We would like to acknowledge the kind assistance of Z. Poláčková with surface oxidation, J. Potměšil with NCD deposition, K. Hruška with SEM imaging, M. Ledinsky with Raman spectroscopy and K. Vyborny with ellipsometry. This research was financially supported by research projects KAN400100701 (GAAV), 202/09/H0041, SVV-2011-263307, P204/10/0212 (GAČR), LC06040 (MŠMT), LC510 (MŠMT), AV0Z10100521 and the Fellowship J.E. Purkyně (ASCR).

References

[1] H. Fudouzi, M. Kobayashi, and N. Shinya, Adv. Mater. 14, 1649 (2002).
[2] W. Wright and D. Chetwynd, Nanotechnology 9, 133 (1998).
[3] P. Mesquida and A. Stemmer, Adv. Mater. 13, 1395 (2001).
[4] H. Jacobs and A. Stemmer, Surf. Interface Anal. 27, 361 (1999).
[5] B. Rezek, T. Mates, J. Stuchlík, J. Kočka, and A. Stemmer, Appl. Phys. Lett. 83, 1764 (2003).
[6] N. Naujoks and A. Stemmer, Microelectron. Eng. 78/79, 331 (2005).
[7] B. Rezek, D. Shin, H. Watanabe, and C. E. Nebel, Sens. Act. B 122, 596 (2007).
[8] B. Rezek, D. Shin, H. Uetsuka, and C. E. Nebel, Phys. Stat. Sol. (a) 204, 2888 (2007).
[9] M. Kalbacova, M. Kalbac, L. Dunsch, A. Kromka, M. Vaněček, B. Rezek, U. Hempel, S. Kmoch Phys. Stat. Sol. (b) 244, 4356 (2007).
[10] A. Kromka, B. Rezek, Z. Remeš, M. Michalka, M. Ledinský, J. Zemek, J. Potměšil, and M. Vaněček, Chem. Vap. Dep. 14, 181 (2008).
[11] C. E. Nebel, Nature Mater. 2, 431 (2003).
[12] S. Koizumi, M. Kamo, Y. Sato, H. Ozaki, and T. Inuzuka, Appl. Phys. Lett. 71, 1065 (1997).
[13] V. Chakrapani, J. C. Angus, A. B. Anderson, S. D. Wolter, B. R. Stoner, G. U. Sumanasekera, Science 318, 1424 (2007).
[14] C. E. Nebel, B. Rezek, D. Shin, H. Watanabe, T. Yamamoto, J. Appl. Phys. 99, 033711 (2006).
[15] P. Bergonzo , D. Tromson and C. Mer, Semicond. Sci. Technol. 18, S105 (2003).
[16] Y. Koide, M. Liao, and J. Alvarez, Diam. Relat. Mater. 15, 1962 (2006).
[17] M. Stallhofer, M. Seifert, M. V. Hauf, G. Abstreiter, M. Stutzmann, J. A. Garrido, and A. W. Holleitner, Appl. Phys. Lett. 97, 111107 (2010).
[18] Y. Sumikawa, T. Banno, K. Kobayashi, Y. Itoh, H. Umezawa, and H. Kawarada, Appl. Phys. Lett. 85, 139 (2004).
[19] J. Čermák, A. Kromka, and B. Rezek, Phys. Stat. Sol. (a) 205, 2136 (2008).
[20] E. Verveniotis, J. Čermák, A. Kromka, and B. Rezek., Phys. Stat. Sol. (b) 246, 2798 (2009).
[21] E. Verveniotis, J. Čermák, A. Kromka, M. Ledinský, Z. Remeš and B. Rezek., Phys. Stat. Sol. (a) 207, 2040 (2010).
[22] E. Verveniotis, J. Čermák, A. Kromka, M. Ledinský, and B. Rezek., Nanoscale Res. Lett. 6, 144 (2011).
[23] B. Rezek, L. Michalíková, E. Ukraintsev, A. Kromka and M. Kalbacova, Sensors 9, 3549 (2009).
[24] B. Rezek and C. E. Nebel, Diam. Relat. Mater. 14, 466 (2005).

[25] B. Rezek J. Stuchlík, J. Kočka, and A. Stemmer, J. Non-Cryst. Solids 351, 3127 (2005).
[26] M. Bartošík, D. Škoda, O. Tomanec, R. Kalousek, P. Jánský, J. Zlámal, J. Spousta, P. Dub, and T. Šikola, Phys. Rev. B 79, 195406 (2009).
[27] R. Singh, S. K. Arora, R. Tyagi, S. K. Agarwal and D. Kanjila, Bull. Mater. Sci. 23, 471 (2000).
[28] D. Häfliger, J. Plitzko and R. Hillenbrand, Appl. Phys. Lett. 85, 4466 (2004).
[29] B. Rezek, J. Stuchlík, A. Fejfar, J. Kočka, J. Appl. Phys. 92, 587 (2002).